Observing spin fractionalization in the Kitaev spin liquid via temperature evolution of indirect resonant inelastic x-ray scattering

Gábor B. Halász, Stefanos Kourtis, Johannes Knolle, and Natalia B. Perkins

Phys. Rev. B **99**, 184417 — Published 15 May 2019

DOI: 10.1103/PhysRevB.99.184417

Observing spin fractionalization in the Kitaev spin liquid via temperature evolution of indirect resonant inelastic x-ray scattering

Gábor B. Halász,[1,2] Stefanos Kourtis,[3] Johannes Knolle,[4] and Natalia B. Perkins[5]

[1] *Materials Science and Technology Division, Oak Ridge National Laboratory, Oak Ridge, TN 37831, USA*
[2] *Kavli Institute for Theoretical Physics, University of California, Santa Barbara, CA 93106, USA*
[3] *Department of Physics, Boston University, Boston, MA 02215, USA*
[4] *Blackett Laboratory, Imperial College London, London SW7 2AZ, United Kingdom*
[5] *School of Physics and Astronomy, University of Minnesota, Minneapolis, MN 55455, USA*

Motivated by the ongoing effort to search for high-resolution signatures of quantum spin liquids, we investigate the temperature dependence of the indirect resonant inelastic x-ray scattering (RIXS) response for the Kitaev honeycomb model. We find that, as a result of spin fractionalization, the RIXS response changes qualitatively at two well-separated temperature scales, T_L and T_H, which correspond to the characteristic energies of the two kinds of fractionalized excitations, $\mathbb{Z}_2$ gauge fluxes and Majorana fermions, respectively. While thermally excited $\mathbb{Z}_2$ gauge fluxes at temperature T_L lead to a general broadening and softening of the response, the thermal proliferation of Majorana fermions at temperature $T_H \sim 10\,T_L$ results in a significant shift of the spectral weight, both in terms of energy and momentum. Due to its exclusively indirect nature, the RIXS process we consider gives rise to a universal magnetic response and, from an experimental perspective, it directly corresponds to the K-edge of Ru^{3+} in the Kitaev candidate material α-$RuCl_3$.

I. INTRODUCTION

Recent years have seen tremendous interest in Kitaev materials[1–9], a family of spin-orbit-assisted Mott insulators on tri-coordinated two-dimensional (2D) and three-dimensional (3D) lattices, in which local, spin-orbit-entangled $j_{\rm eff} = 1/2$ moments interact via strongly bond-directional Ising-like interactions. The most extensively studied Kitaev materials are the iridates A_2IrO_3 (A = Li, Na)[10–19] and $H_3LiIr_2O_6$[20], and the ruthenium compound α-$RuCl_3$[21–24]. The interest in these materials originates from the belief that they are proximate to the Kitaev quantum spin liquid (QSL)[1] due to the presence of dominant Kitaev interactions in their microscopic Hamiltonians[18,25–31].

When searching for QSL physics in Kitaev materials, a general feature to look for is the fractionalization of spins into two types of quasiparticle excitations, according to the exact solution of the Kitaev model[1]: localized, gapped $\mathbb{Z}_2$ fluxes and itinerant, gapless Majorana fermions. In pursuit of spin fractionalization, a lot of experimental and theoretical effort has been devoted to the study of spin dynamics in Kitaev materials through various dynamical probes, such as inelastic neutron scattering (INS)[32–41], Raman scattering[42–49], and resonant inelastic x-ray scattering (RIXS)[50,51]. The key idea is that, even if residual magnetic order sets in below a critical temperature, which indeed happens in most of the Kitaev materials, the fractionalized quasiparticles of the nearby QSL phase may still lead to observable signatures in the dynamical response[36,52].

In particular, there is a growing body of experimental evidence that the ground state of the spin-orbit-assisted honeycomb Mott insulator α-$RuCl_3$ is proximate to the Kitaev QSL phase, despite the fact that it exhibits zigzag antiferromagnetic order below $T_N \simeq 7$ K[21–24]. For example, the INS response of α-$RuCl_3$[36,39,40] shows a broad continuum spectrum of 2D magnetic fluctuations around the center of the Brillouin zone, which is indicative of spin fractionalization and is in agreement with the corresponding theoretical prediction for the Kitaev honeycomb model[33,34]. Promising results were also obtained by Raman scattering experiments in α-$RuCl_3$, detecting

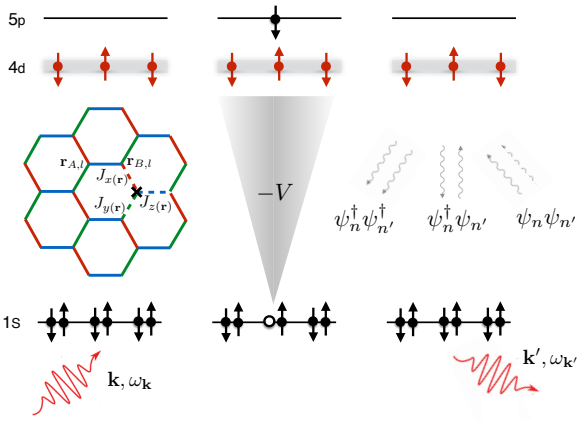

FIG. 1. Illustration of an indirect RIXS process at the Ru^{3+} K-edge creating Majorana fermion excitations in the Kitaev honeycomb model, due to the local modification of magnetic couplings in the intermediate state. The three bond types x, y, and z of the lattice are marked by red, green, and blue, respectively, while the bonds with modified couplings $J_{\kappa(\mathbf{r})}$ between the photon-scattering site $\mathbf{r}$ and the neighboring sites $\kappa(\mathbf{r})$ (with $\kappa = x, y, z$) are denoted by dashed lines. The incoming (outgoing) x-ray photons have momenta $\mathbf{k}$ ($\mathbf{k}'$) and energies $\omega_{\mathbf{k}} = c|\mathbf{k}|$ ($\omega_{\mathbf{k}'} = c|\mathbf{k}'|$). At finite temperature, three kinds of indirect RIXS processes contribute to the response: Stokes processes creating two fermions, anti-Stokes processes annihilating two fermions, and "mixed" processes creating one fermion while annihilating another one.

a broad continuum below 100 K that even persists into the magnetically ordered phase[43,45]. Moreover, the temperature dependence of the Raman spectral weight can be interpreted in terms of the spins fractionalizing into fermionic quasiparticles[49].

As a general spectroscopic probe of magnetic materials, RIXS has important advantages over both INS and Raman scattering. In contrast to INS, which only measures dynamic single-spin correlations, and Raman scattering, which is restricted to essentially zero momentum due to its low-energy photons, RIXS offers greater versatility in measuring a wider range of dynamic correlations with full momentum resolution[53–56]. Specifically, for the Kitaev QSL, it was predicted by some of us that the magnetic channels of RIXS are capable of picking up both types of fractionalized excitations[50,51]. Indeed, while the non-spin-conserving channels are dominated by the localized $\mathbb{Z}_2$ fluxes and thus give rise to a weakly dispersive response, the spin-conserving channel couples exclusively to the Majorana fermions and can effectively probe the characteristic graphene-like dispersion of these exotic fractionalized quasiparticles.

Nevertheless, spin fractionalization in the Kitaev materials has not yet been observed in RIXS experiments due to at least two major difficulties in designing a suitable measurement. First, in order to distinguish between the various magnetic channels, one would need to do polarization analysis on the outgoing x-ray beam. Second, the energy resolution of RIXS at the previously proposed L_3-edge[50,51] is rather poor, both in the iridates and in α-$RuCl_3$. In this work, we instead propose that signatures of fractionalized excitations in α-$RuCl_3$ can be probed by *indirect* RIXS at the K-edge of Ru^{3+}. In addition to a favorable predicted energy resolution[57,58], this edge has only one magnetic channel due to its indirect nature, and the corresponding magnetic response is thus independent of x-ray polarization.

Furthermore, it is now well appreciated that, due to the flat band of low-energy $\mathbb{Z}_2$ fluxes, the dynamical responses of the Kitaev QSL are rather sensitive to thermal fluctuations. Indeed, already at temperatures corresponding to only a small fraction of the Kitaev exchange energy, thermal population of the fluxes[59] can give rise to finite-temperature responses that are strikingly different from their zero-temperature counterparts[60–63]. To provide a useful guide for experimentalists, we therefore calculate the indirect RIXS response of the Kitaev QSL at *finite temperature* and describe how the temperature evolution of this response reflects the spin-fractionalization scheme in the Kitaev QSL.

Our main result is that there are qualitative changes in the RIXS response at two distinct temperature scales, T_L and T_H, separated by an order of magnitude, which correspond to the characteristic energies of the $\mathbb{Z}_2$ fluxes and the Majorana fermions, respectively. At the scale of T_L, the fluxes become thermally excited and give rise to an effective disorder for the Majorana fermions, thereby leading to an overall *broadening* of the response as well as the softening of the quasi-sharp features present at zero temperature. At the scale of $T_H \sim 10\,T_L$, the Majorana fermions become excited in large numbers, leading to an overall *shift* of the spectral weight, both from positive to negative energies and from the boundary to the center of the Brillouin zone. In the high-temperature regime, we also identify a pronounced peak in the spectral weight around zero energy and momentum, corresponding to collective energy-density fluctuations, and we argue that this peak is related to the quasi-elastic peak in the experimental Raman response of α-$RuCl_3$[43,49].

II. INDIRECT RIXS IN THE KITAEV QUANTUM SPIN LIQUID

In RIXS experiments, core electrons of a specific ion are promoted to an unoccupied state using an x-ray beam, thereby locally exciting the irradiated material into a highly energetic and very short-lived (~ 1 fs) intermediate state. Motivated by α-$RuCl_3$, we are interested in RIXS processes at the K-edge of Ru^{3+} (see Fig. 1), which involve the excitation of an electron from the $1s$ core shell into an unoccupied $5p$ state *above* the $4d$ valence shell. Since no electrons are excited directly into the valence orbitals, magnetic excitations can only be created by *indirect* RIXS processes, which do not change the spin of the valence shell and thus correspond to the spin-conserving channel discussed in Refs. 50 and 51. Consequently, the K-edge of Ru^{3+} has only one magnetic RIXS channel, giving rise to a universal magnetic response that does not depend on the x-ray polarizations.

In α-$RuCl_3$, the magnetism of each Ru^{3+} ion is governed by a $j_{\text{eff}} = 1/2$ Kramers doublet in the t_{2g} orbitals of the $4d$ valence shell[2], and we assume that the effective low-energy Hamiltonian acting on these Kramers doublets is that of the Kitaev model[1]:

$$H = -J \sum_{\langle \mathbf{r},\mathbf{r}'\rangle_x} \sigma^x_{\mathbf{r}} \sigma^x_{\mathbf{r}'} - J \sum_{\langle \mathbf{r},\mathbf{r}'\rangle_y} \sigma^y_{\mathbf{r}} \sigma^y_{\mathbf{r}'} - J \sum_{\langle \mathbf{r},\mathbf{r}'\rangle_z} \sigma^z_{\mathbf{r}} \sigma^z_{\mathbf{r}'}, \quad (1)$$

where the three bond types $\kappa = x, y, z$ are distinct in their orientations (see Fig. 1). Using the Kitaev fermionization $\sigma^\kappa_{\mathbf{r}} = i b^\kappa_{\mathbf{r}} c_{\mathbf{r}}$, this Hamiltonian can be written as $H = J \sum_\kappa \sum_{\langle \mathbf{r},\mathbf{r}'\rangle_\kappa} i u^\kappa_{\mathbf{r},\mathbf{r}'} c_{\mathbf{r}} c_{\mathbf{r}'}$ in terms of the Majorana fermions $b^\kappa_{\mathbf{r}}$ and $c_{\mathbf{r}}$, where $u^\kappa_{\mathbf{r},\mathbf{r}'} \equiv i b^\kappa_{\mathbf{r}} b^\kappa_{\mathbf{r}'}$. Importantly, $u^\kappa_{\mathbf{r},\mathbf{r}'}$ are commuting constants of motion, and they give rise to static flux degrees of freedom $\Pi_{\langle \mathbf{r},\mathbf{r}'\rangle \in p} u^\kappa_{\mathbf{r},\mathbf{r}'} = \pm 1$ at the plaquettes p. Moreover, in each flux sector characterized by $u^\kappa_{\mathbf{r},\mathbf{r}'} = \pm 1$, one obtains a free-fermion Hamiltonian for $c_{\mathbf{r}}$, which can thus be identified as deconfined Majorana-fermion excitations. Since there are no flux excitations in the ground state, it belongs to the flux sector with $\Pi_{\langle \mathbf{r},\mathbf{r}'\rangle \in p} u^\kappa_{\mathbf{r},\mathbf{r}'} = +1$ for all p.

During the RIXS process, a momentum $\mathbf{q} = \mathbf{k} - \mathbf{k}'$ and an energy $\omega = \omega_{\mathbf{k}} - \omega_{\mathbf{k}'} = c\,\{|\mathbf{k}| - |\mathbf{k}'|\}$ is transferred into the Kitaev QSL, where $\mathbf{k}$ and $\mathbf{k}'$ are the momenta of the incoming and the outgoing x-ray photons, respectively (see Fig. 1). In the intermediate state, the $1s$ core hole

acts like a nonmagnetic impurity and locally modifies (i.e., strengthens or weakens) the coupling strength J of the effective Kitaev model[64]. The intermediate state is then an eigenstate $|\tilde{n}_{\mathbf{r}}\rangle$ of the perturbed Kitaev model

$$\tilde{H}_{\mathbf{r}} = H - \delta J \sum_{\kappa=x,y,z} \sigma^{\kappa}_{\mathbf{r}} \sigma^{\kappa}_{\kappa(\mathbf{r})}, \tag{2}$$

where $\kappa(\mathbf{r})$ is the site connected to the core-hole site $\mathbf{r}$ by a κ bond. Note that the change in the Kitaev coupling strength, δJ, may be positive or negative and that the limit of a nonmagnetic vacancy[65–67], corresponding to, for example, the L-edges of Ru^{3+} or Ir^{4+}[50,51], is recovered by setting $\delta J = -J$.

Due to the indirect nature of the RIXS process considered, the Kramers-Heisenberg formula[53] for the RIXS vertex takes the simplified form

$$R(\mathbf{q}) = \sum_{\mathbf{r}} e^{i\mathbf{q}\cdot\mathbf{r}} \sum_{\tilde{n}_{\mathbf{r}}} \frac{|\tilde{n}_{\mathbf{r}}\rangle\langle\tilde{n}_{\mathbf{r}}|}{\Omega - E_{\tilde{n}} + i\Gamma}\,, \tag{3}$$

where Γ is the core-hole decay rate, $E_{\tilde{n}}$ is the energy of the intermediate state $|\tilde{n}_{\mathbf{r}}\rangle$, and Ω is the energy of the incoming x-ray photon with respect to the K-edge resonance energy. Considering the experimentally relevant fast-collision regime, where $J \ll \Gamma$, we may assume that resonance is close enough, such that $\Omega \ll \Gamma$, and expand Eq. (3) in $(\Omega - E_{\tilde{n}})/\Gamma$ up to the order of $1/\Gamma^2$. Exploiting $\sum_{\tilde{n}_{\mathbf{r}}} |\tilde{n}_{\mathbf{r}}\rangle\langle\tilde{n}_{\mathbf{r}}| = 1$ as well as $\sum_{\tilde{n}_{\mathbf{r}}} E_{\tilde{n}} |\tilde{n}_{\mathbf{r}}\rangle\langle\tilde{n}_{\mathbf{r}}| = \tilde{H}_{\mathbf{r}}$, and neglecting any terms giving rise to exclusively elastic responses, the lowest-order RIXS vertex then becomes

$$R(\mathbf{q}) = \frac{\delta J}{\Gamma^2} \sum_{\mathbf{r}} e^{i\mathbf{q}\cdot\mathbf{r}} \sum_{\kappa} \sigma^{\kappa}_{\mathbf{r}} \sigma^{\kappa}_{\kappa(\mathbf{r})}. \tag{4}$$

This result has a straightforward physical interpretation: the indirect RIXS vertex in Eq. (4) is due to additional exchange interactions of strength δJ that are temporarily switched on around the core-hole site $\mathbf{r}$ in the short-lived (lifetime: $\tau \sim 1/\Gamma$) intermediate state[68].

III. FINITE-TEMPERATURE RESPONSE

The main result of this work is the calculation of the RIXS response at finite temperature, which first requires a finite-temperature formulation of the underlying Kitaev model[59–63]. Qualitatively, thermal spin fractionalization in the Kitaev model manifests itself in successive entropy releases at two well-separated temperature scales T_L and T_H. At low temperatures ($T \ll T_L$), the fluxes are completely frozen and only a small number of Majorana fermions are thermally excited. At intermediate temperatures ($T_L \lesssim T \lesssim T_H$), thermal energy goes into both fluxes and Majorana fermions, but their fractionalized nature remains readily observable. Finally, at high temperatures ($T \gg T_H$), fluxes and Majorana fermions recombine into spins, and the system crosses over to a conventional paramagnetic regime.

Instead of a full and numerically costly Monte-Carlo sampling of flux excitations[59], a quantitative approximation of the finite-temperature behavior is obtained by taking a random average over "typical" flux sectors and solving the free-fermion problem in each flux sector exactly[69]. Each "typical" flux sector at temperature T is obtained by creating two flux excitations around each bond with probability P_T such that the resulting probability of a flux excitation at any plaquette is

$$\frac{1-(1-2P_T)^6}{2} = f_T(\Delta) \equiv \frac{1}{1+\exp(\Delta/T)}\,, \tag{5}$$

where $\Delta \approx 0.15J$ is the single-flux gap. The solution for this probability is given by

$$P_T = \frac{1-[1-2f_T(\Delta)]^{1/6}}{2}\,. \tag{6}$$

In each "typical" flux sector, the free-fermion Hamiltonian then takes the form

$$\mathcal{H} = J \sum_{\kappa} \sum_{\langle \mathbf{r},\mathbf{r}'\rangle_{\kappa}} i\bar{u}_{\mathbf{r},\mathbf{r}'} c_{\mathbf{r}} c_{\mathbf{r}'}, \tag{7}$$

where each $\bar{u}_{\mathbf{r},\mathbf{r}'} \equiv \langle u^{\kappa}_{\mathbf{r},\mathbf{r}'}\rangle$ is $+1$ with probability $1-P_T$ and -1 with probability P_T.

Exploiting the bipartite nature of the honeycomb lattice, and noting that each unit cell l has two sites $\mathbf{r}_{A,l}$ and $\mathbf{r}_{B,l}$ in the two sublattices A and B, this free-fermion Hamiltonian can be written as $\mathcal{H} = \sum_{l,l'} iM_{ll'} c_{A,l} c_{B,l'}$, where $M_{ll'} = J\bar{u}_{\mathbf{r}_{A,l},\mathbf{r}_{B,l'}}$ if $\mathbf{r}_{A,l}$ and $\mathbf{r}_{B,l'}$ are connected and $M_{ll'} = 0$ otherwise. Note also that $c_{A,l} \equiv c_{\mathbf{r}_{A,l}}$ and $c_{B,l} \equiv c_{\mathbf{r}_{B,l}}$. Finally, the free-fermion Hamiltonian is recast into the canonical form $\mathcal{H} = \sum_n \varepsilon_n(\psi^{\dagger}_n\psi_n - 1/2)$, where the fermions $\psi_n = (\gamma_{A,n} + i\gamma_{B,n})/2$, in terms of $\gamma_{A,n} = \sum_l U_{ln} c_{A,l}$ and $\gamma_{B,n} = \sum_l V_{ln} c_{B,l}$, and their energies $\varepsilon_n = 2\Lambda_{nn}$ are obtained from the singular-value decomposition $M = U \cdot \Lambda \cdot V^T$[70].

In any given flux sector, the lowest-order RIXS vertex in Eq. (4) can be expressed in terms of the fermions as

$$\begin{aligned}\mathcal{R}(\mathbf{q}) &= -\frac{\delta J}{J\Gamma^2} \sum_{l,l'} iM_{ll'} c_{A,l} c_{B,l'} \left(e^{i\mathbf{q}\cdot\mathbf{r}_{A,l}} + e^{i\mathbf{q}\cdot\mathbf{r}_{B,l'}}\right) \\ &\propto \sum_{n,n'} \left(\psi_n + \psi^{\dagger}_n\right)\left(\psi_{n'} - \psi^{\dagger}_{n'}\right) \\ &\qquad \times \left[W_A(\mathbf{q})\cdot\Lambda + \Lambda\cdot W_B(\mathbf{q})\right]_{nn'}\,,\end{aligned} \tag{8}$$

where we introduce $[S_{A/B}(\mathbf{q})]_{ll'} \equiv \delta_{ll'} e^{i\mathbf{q}\cdot\mathbf{r}_{A/B,l}}$ as well as $W_A(\mathbf{q}) \equiv U^T \cdot S_A(\mathbf{q}) \cdot U$ and $W_B(\mathbf{q}) \equiv V^T \cdot S_B(\mathbf{q}) \cdot V$. Finally, by neglecting all elastic terms that do not change any fermion numbers and separating inelastic terms that change fermion numbers in inequivalent ways, the RIXS vertex in Eq. (8) can be written as

$$\mathcal{R}(\mathbf{q}) \propto \sum_{n<n'} \left[\mathcal{R}^{(1)}_{nn'}(\mathbf{q}) + \mathcal{R}^{(2)}_{nn'}(\mathbf{q})\right] + \sum_{n\neq n'} \mathcal{R}^{(3)}_{nn'}. \tag{9}$$

In particular, the first term describes Stokes processes creating two fermions each:

$$\mathcal{R}^{(1)}_{nn'}(\mathbf{q}) = -\psi^\dagger_n \psi^\dagger_{n'} [\mathcal{A}_-(\mathbf{q})]_{nn'}, \tag{10}$$

the second term describes anti-Stokes processes annihilating two fermions each:

$$\mathcal{R}^{(2)}_{nn'}(\mathbf{q}) = \psi_n \psi_{n'} [\mathcal{A}_-(\mathbf{q})]_{nn'}, \tag{11}$$

and the third term describes "mixed" processes creating one fermion and annihilating one fermion each:

$$\mathcal{R}^{(3)}_{nn'}(\mathbf{q}) = \psi^\dagger_n \psi_{n'} [\mathcal{A}_+(\mathbf{q})]_{nn'}, \tag{12}$$

where $\mathcal{A}_\pm(\mathbf{q}) = \{W_A(\mathbf{q}) \pm W_B(\mathbf{q}), \Lambda\}_\pm$ in terms of the (anti)commutator $\{a, b\}_\pm \equiv a \cdot b \pm b \cdot a$.

At finite temperature T, the resulting RIXS intensity of any given flux sector is given by Fermi's golden rule:

$$\mathcal{I}(\omega, \mathbf{q}) = \sum_{m,m'} \frac{e^{-E_m/T}}{Z} \left| \langle m' | \mathcal{R}(\mathbf{q}) | m \rangle \right|^2 \delta(\omega + E_m - E_{m'}), \tag{13}$$

where $Z \equiv \sum_m e^{-E_m/T}$ is the partition function. Importantly, the free-fermion eigenstates $|m\rangle = \prod_n (\psi^\dagger_n)^{N_n} |0\rangle$ with energies $E_m = \sum_n N_n \varepsilon_n$ are labeled by the fermion occupation numbers $N_n = \{0, 1\}$. Since the various terms in Eq. (9) all change the fermion numbers in inequivalent ways, there can be no interference between them in Eq. (13) and their corresponding intensities can be calculated independently. Moreover, since the fermions do not interact, the matrix elements of the terms $\mathcal{R}^{(1,2,3)}_{nn'}(\mathbf{q})$ only depend on the fermions n and n' whose numbers they actually change. Substituting Eq. (9) into Eq. (13), the lowest-order RIXS intensity is then

$$\begin{aligned}
\mathcal{I}(\omega, \mathbf{q}) &\propto \mathcal{I}^{(1)}(\omega, \mathbf{q}) + \mathcal{I}^{(2)}(\omega, \mathbf{q}) + \mathcal{I}^{(3)}(\omega, \mathbf{q}), \\
\mathcal{I}^{(1)}(\omega, \mathbf{q}) &= \sum_{n<n'} \left[1 - f_T(\varepsilon_n)\right] \left[1 - f_T(\varepsilon_{n'})\right] |\mathcal{A}_-(\mathbf{q})|^2_{nn'} \, \delta(\omega - \varepsilon_n - \varepsilon_{n'}), \\
\mathcal{I}^{(2)}(\omega, \mathbf{q}) &= \sum_{n<n'} f_T(\varepsilon_n) f_T(\varepsilon_{n'}) \, |\mathcal{A}_-(\mathbf{q})|^2_{nn'} \, \delta(\omega + \varepsilon_n + \varepsilon_{n'}), \\
\mathcal{I}^{(3)}(\omega, \mathbf{q}) &= \sum_{n \neq n'} \left[1 - f_T(\varepsilon_n)\right] f_T(\varepsilon_{n'}) \, |\mathcal{A}_+(\mathbf{q})|^2_{nn'} \, \delta(\omega - \varepsilon_n + \varepsilon_{n'}),
\end{aligned} \tag{14}$$

where the three distinct terms correspond to Stokes, anti-Stokes, and "mixed" processes, respectively. In the limit of $T \to 0$, the Fermi functions $f_T(\varepsilon_n)$ vanish for $\varepsilon_n > 0$, implying that only Stokes processes are allowed.

In principle, the finite-temperature RIXS intensity of the Kitaev model is obtained by taking an average of the intensities corresponding to randomly selected "typical" flux sectors: $I(\omega, \mathbf{q}) = \overline{\mathcal{I}(\omega, \mathbf{q})}$. For large enough system sizes, however, there are no observable differences between the intensities of the individual flux sectors. In practice, it is therefore sufficient to approximate the average intensity with the intensity corresponding to *any* "typical" flux sector: $I(\omega, \mathbf{q}) = \mathcal{I}(\omega, \mathbf{q})$.

IV. RESULTS AND DISCUSSION

The lowest-order RIXS intensity $I(\omega, \mathbf{q})$ is plotted in Figs. 2 and 3 for a range of different temperatures T, along an entire high-symmetry path and at specific high-symmetry points of the Brillouin zone, respectively. We start by briefly discussing the limit of zero temperature[50], in which case the fermions $\psi_n \equiv \psi_{\mathbf{k}}$ are labeled by their momenta $\mathbf{k}$, and the matrix element $|\mathcal{A}_-(\mathbf{q})|_{\mathbf{k},\mathbf{k}'}$ in Eq. (14) vanishes unless $\mathbf{q} = \mathbf{k} + \mathbf{k}'$. The RIXS intensity $I(\omega, \mathbf{q}) \propto \sum_{\mathbf{k}} |\mathcal{A}_-(\mathbf{q})|^2_{\mathbf{k},\mathbf{q}-\mathbf{k}} \, \delta(\omega - \varepsilon_{\mathbf{k}} - \varepsilon_{\mathbf{q}-\mathbf{k}})$ can then be understood in terms of the characteristic momentum dispersion $\varepsilon_{\mathbf{k}}$ of the fermions[50,51].

Ignoring the matrix element $[\mathcal{A}_-(\mathbf{q})]_{\mathbf{k},\mathbf{q}-\mathbf{k}}$, the RIXS intensity at each momentum $\mathbf{q}$ is proportional to the joint density of states $\hat{g}_\omega(\mathbf{q}) = \sum_{\mathbf{k}} \delta(\omega - \varepsilon_{\mathbf{k}} - \varepsilon_{\mathbf{q}-\mathbf{k}})$, which in turn corresponds to an effective (joint) band dispersion $\hat{\varepsilon}_{\mathbf{k}}(\mathbf{q}) \equiv \varepsilon_{\mathbf{k}} + \varepsilon_{\mathbf{q}-\mathbf{k}}$ as a function of the fermion momentum $\mathbf{k}$. Due to the finite width of this effective band, the RIXS intensity is nonzero for a finite energy range at each momentum $\mathbf{q}$, which can be identified as an indirect signature of fractionalization[50]. However, while truly sharp features $I(\omega, \mathbf{q}) \propto \delta(\omega - \hat{\omega}_{\mathbf{q}})$ are absent from the RIXS response, there are clear quasi-sharp features $I(\omega, \mathbf{q}) \propto -\log(\omega - \hat{\omega}_{\mathbf{q}})$ [see Fig. 3] due to logarithmic divergences in $\hat{g}_\omega(\mathbf{q})$, which correspond to van Hove singularities of the effective band $\hat{\varepsilon}_{\mathbf{k}}(\mathbf{q})$.

As the temperature is increased, there are qualitative changes in the RIXS response at the two characteristic temperature scales $T_L \approx \Delta$ and $T_H \approx J$, which can be identified as indirect signatures of the flux and fermion excitations, respectively. At temperatures $T \gtrsim T_L$, thermally excited fluxes behave like disorder from the perspective of the fermions[69], and fermion momentum is therefore no longer a good quantum number. As a result

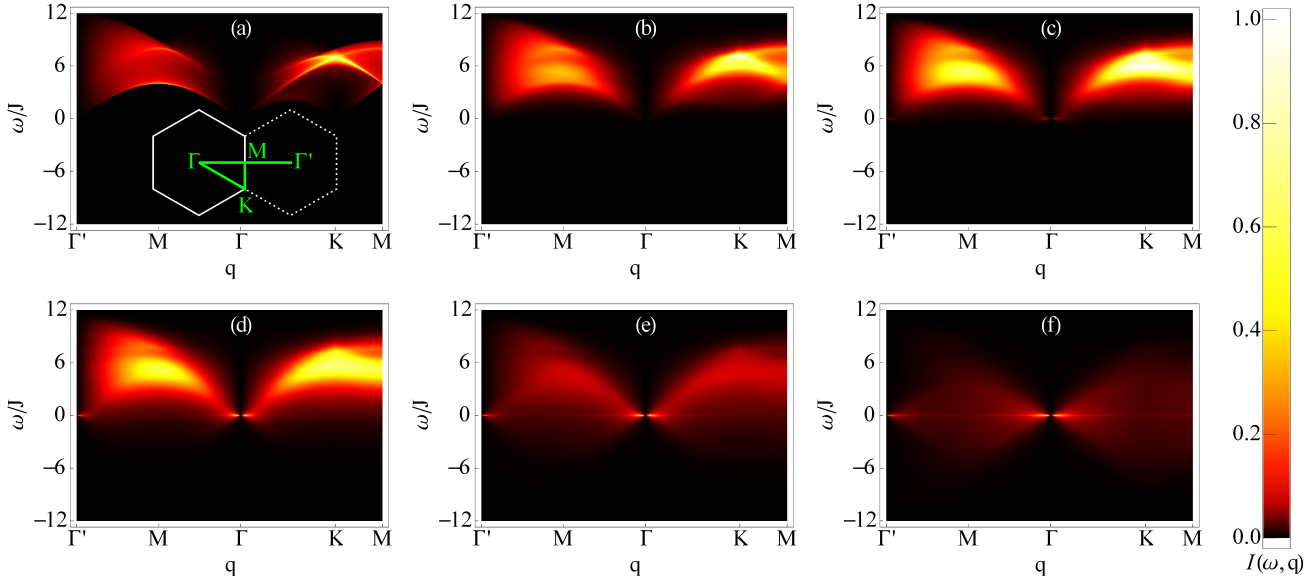

FIG. 2. Temperature evolution of the indirect RIXS response for the Kitaev honeycomb model. The lowest-order RIXS intensity $I(\omega, \mathbf{q})$ is plotted for temperatures (a) $T = 0$, (b) $T = 0.1J$, (c) $T = 0.2J$, (d) $T = 0.5J$, (e) $T = J$, and (f) $T = 5J$ along the high-symmetry path Γ'-M-Γ-K-M in the Brillouin zone [marked by green line in the inset of subfigure (a)].

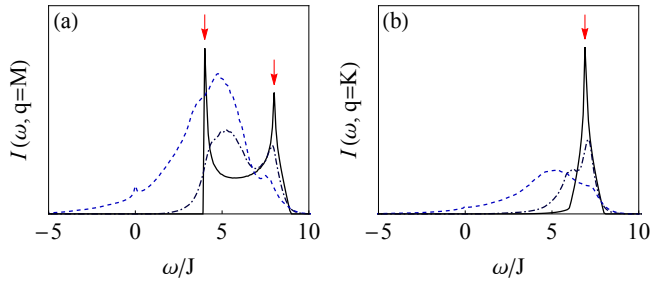

FIG. 3. Lowest-order RIXS intensities $I(\omega, \mathbf{q})$ at the M point (a) and at the K point (b) of the Brillouin zone for temperatures $T = 0$ (solid line), $T = 0.1J$ (dashed-dotted line), and $T = J$ (dashed line). Red arrows indicate quasi-sharp features (i.e., logarithmic divergences) at $T = 0$.

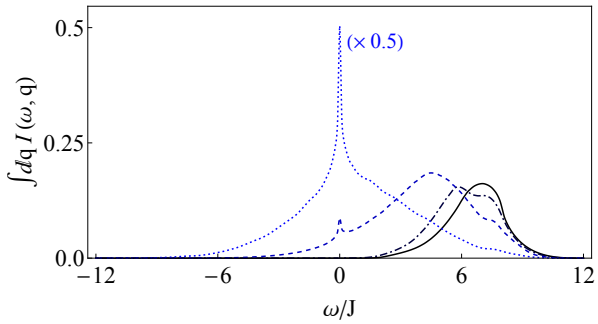

FIG. 4. Momentum-integrated RIXS intensity $I(\omega)$ for temperatures $T = 0$ (solid line), $T = 0.1J$ (dashed-dotted line), $T = J$ (dashed line), and $T = 5J$ (dotted line). The $T = 5J$ curve is multiplied by 0.5 to compare with other curves.

of this effective disorder, the quasi-sharp features of the zero-temperature RIXS response disappear. Also, in the absence of a momentum selection rule (e.g., $\mathbf{q} = \mathbf{k} + \mathbf{k}'$), a larger number of processes become allowed and hence the energy range of the RIXS response increases. Interestingly, both of these features are already observable at $T = 0.1J \lesssim \Delta$ (see Figs. 2 and 3).

At temperatures $T \gtrsim T_H$, fermions become thermally excited in large numbers, and Stokes processes are thus no longer dominant over anti-Stokes and "mixed" processes. Consequently, the spectral weight of the RIXS response is shifted to lower energies and becomes nonzero even at $\omega < 0$. To distinguish this overall shift of the spectral weight from the finer changes discussed in the previous paragraph, we plot the momentum-integrated RIXS intensity $I(\omega) \equiv \int d\mathbf{q}\, I(\omega, \mathbf{q})$ for a range of different temperatures in Fig. 4. While the $T = 0.1J$ response is almost identical to the zero-temperature one, the spectral weights of the $T \geq J$ responses are significantly shifted to progressively smaller energies. In particular, the $T = 5J$ response is almost symmetric with respect to $\omega = 0$, indicating that Stokes and anti-Stokes processes are almost equally probable.

Moreover, at temperatures $T \gg T_H$, the momentum-integrated RIXS intensity exhibits a strong peak around zero energy as a result of quasi-elastic "mixed" processes at small momenta $\mathbf{q}$. These processes do not change the total number of fermions and instead correspond to collective energy-density fluctuations[71–73]. In Fig. 5, we pinpoint the existence of these quasi-elastic processes in two different ways. First, we plot the energy-integrated RIXS intensity $I(\mathbf{q}) \equiv \int d\omega\, I(\omega, \mathbf{q})$ in Fig. 5(a), and observe that its maximum is transferred from the boundary to the center of the Brillouin zone upon increasing the

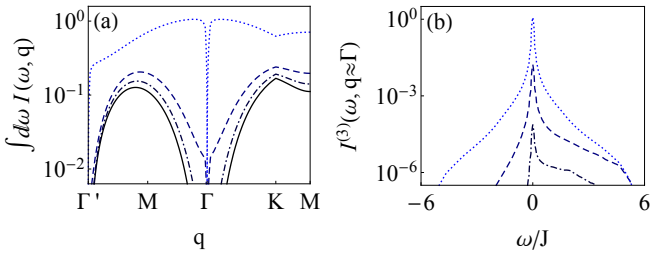

FIG. 5. (a) Energy-integrated RIXS intensity $I(\mathbf{q})$ along the high-symmetry path Γ'-M-Γ-K-M [see inset of Fig. 2(a)] and (b) "mixed" RIXS intensity $I^{(3)}(\omega, \mathbf{q})$ in a small region around the Γ point. In each subfigure, the curves correspond to temperatures $T = 0$ (solid line), $T = 0.1J$ (dashed-dotted line), $T = 0.5J$ (dashed line), and $T = 5J$ (dotted line), and are normalized such that the peak of the $T = 5J$ curve is at 1.

temperature. Second, we plot the "mixed" component of the RIXS intensity, corresponding to the third term in Eq. (14), integrated over a small region around the Γ point of the Brillouin zone, in Fig. 5(b). This quantity, $I^{(3)}(\omega, \mathbf{q} \approx \Gamma) \equiv \int_{|\mathbf{q}|<\epsilon} d\mathbf{q}\, I^{(3)}(\omega, \mathbf{q})$, is strongly peaked around zero energy, and its $\omega = 0$ peak grows rapidly as the temperature is increased[74]. Interestingly, such a quasi-elastic peak has been experimentally observed at high temperatures in the Raman response of the Kitaev QSL candidate α-$RuCl_3$[43,49].

We emphasize that the matrix elements $[\mathcal{A}_\pm(\mathbf{q})]_{nn'}$ in Eq. (14) also lead to observable features in the RIXS response. First of all, the RIXS intensity $I(\omega, \mathbf{q})$ vanishes for all energies ω at a reciprocal lattice vector $\mathbf{q} = \mathbf{G}$ or, equivalently, at the Γ point of the Brillouin zone. Indeed, since the RIXS vertex $R(\mathbf{G})$ in Eq. (4) is proportional to the Hamiltonian H in Eq. (1), it does not create any excitations and gives rise to a purely elastic response. Importantly, this connection between H and $R(\mathbf{G})$ is valid on the level of the spins, and the corresponding suppression around the Γ point is thus a robust feature of the RIXS response at arbitrary temperature[75].

Furthermore, in comparison to the equivalent Γ' points in the neighboring Brillouin zones ($\mathbf{q} = \mathbf{G} \neq \mathbf{0}$), the suppression of the RIXS response may be stronger or weaker around the Γ point in the central Brillouin zone ($\mathbf{q} = \mathbf{0}$) [see Fig. 2] due to a destructive or constructive interference between RIXS processes at the two sublattices of the bipartite honeycomb lattice. In general, there is a complex phase factor $\pm i$ between the two sublattices for each fermion created (annihilated). For the (anti-)Stokes processes, dominating at low temperatures and/or far away from $\omega = 0$, the interference at $\mathbf{q} = \mathbf{0}$ is destructive due to $(\pm i)^2 = -1$, and the RIXS response is *weaker* around the central Γ point. Conversely, for the "mixed" processes, dominating close to $\omega = 0$ at high temperatures, the interference at $\mathbf{q} = \mathbf{0}$ is constructive due to $(+i)(-i) = +1$, and the RIXS response is *stronger* around the central Γ point. Importantly, the phase factors $\pm i$ indicate that inversion symmetry acts projectively on the fermions, and the stronger suppression around the central Γ point at low temperatures $T \lesssim T_L$ is thus an indirect signature of their fractionalized nature[50,51].

V. SUMMARY AND OUTLOOK

In this work, we presented a microscopic calculation of the finite-temperature RIXS response for the Kitaev QSL on the honeycomb lattice. In order to obtain a universal magnetic response, we concentrated on indirect RIXS which only has one magnetic channel and couples exclusively to the Majorana fermions. However, in stark contrast with the case of zero temperature, thermally excited $\mathbb{Z}_2$ fluxes are also indirectly observable at finite temperature as they give rise to an effective disorder potential for the Majorana fermions. In fact, as the temperature is increased, the RIXS response changes qualitatively at two well-separated temperature scales, T_L and T_H, due to the thermal proliferation of $\mathbb{Z}_2$ fluxes and Majorana fermions, respectively. We thus conclude that the temperature evolution of the RIXS response provides further evidence of spin fractionalization, in addition to those already observable at zero temperature.

Moreover, as the small-momentum regime of RIXS is directly related to Raman scattering, we can provide a possible explanation for the strong quasi-elastic peak that has been experimentally observed in the Raman response of α-$RuCl_3$[43,49]. Indeed, we found a similar quasi-elastic peak in our theoretical RIXS response above the higher temperature scale T_H and understood that it corresponds to long-wavelength collective fluctuations of the Majorana fermions. While we were not able to quantitatively reproduce its experimentally observed temperature dependence, we argue that this strong quasi-elastic peak, which so far has been subtracted as an unknown background, is also qualitatively consistent with the presence of fractionalized excitations in α-$RuCl_3$.

Finally, we emphasize that our results capture the fundamental properties of the indirect RIXS process at the K-edge of Ru^{3+} in α-$RuCl_3$. The predicted energy resolution at this edge, $\Delta\omega \sim 1$ meV[57,58], is much smaller than the bandwidth $12J \sim 20$ meV[29] of the magnetic RIXS response. Due to this favorable prediction for the energy resolution and the universality of the corresponding RIXS response, we hope that, in the near future, the quantitative predictions in this work will serve as a useful guide for RIXS experiments in Kitaev materials.

ACKNOWLEDGMENTS

We are grateful to K. Burch and J. H. Kim for valuable discussions. The work of G. B. H. was supported at ORNL by Laboratory Director's Research and Development funds and at the KITP by the Gordon and Betty Moore Foundation's EPiQS Initiative through Grant No. GBMF4304. S. K. was supported in part through

the Boston University Center for Non-Equilibrium Systems and Computation. N. B. P. was supported by the U.S. Department of Energy, Office of Science, Basic Energy Sciences under Award DE-SC0018056.

[1] A. Kitaev, Annals of Physics **321**, 2 (2006).
[2] G. Jackeli and G. Khaliullin, Phys. Rev. Lett. **102**, 017205 (2009).
[3] J. Chaloupka, G. Jackeli, and G. Khaliullin, Phys. Rev. Lett. **105**, 027204 (2010).
[4] G. Cao and L. DeLong, eds., *Frontiers of 4d- and 5d-Transition Metal Oxides* (World Scientific Publishing Co. Pte. Ltd., 2013).
[5] W. Witczak-Krempa, G. Chen, Y. B. Kim, and L. Balents, Ann. Rev. Cond. Matt. Phys. **5**, 57 (2014).
[6] J. G. Rau, E. K.-H. Lee, and H.-Y. Kee, Ann. Rev. Cond. Matt. Phys. **7**, 195 (2016).
[7] S. Trebst, arXiv:1701.07056 (2017).
[8] M. Hermanns, I. Kimchi, and J. Knolle, Annu. Rev. Condens. Matter Phys. **9**, 17 (2018).
[9] S. M. Winter, A. A. Tsirlin, M. Daghofer, J. van den Brink, Y. Singh, P. Gegenwart, and R. Valenti, J. Phys.: Condens. Matter **29**, 493002 (2017).
[10] Y. Singh and P. Gegenwart, Phys. Rev. B **82**, 064412 (2010).
[11] X. Liu, T. Berlijn, W.-G. Yin, W. Ku, A. Tsvelik, Y.-J. Kim, H. Gretarsson, Y. Singh, P. Gegenwart, and J. P. Hill, Phys. Rev. B **83**, 220403 (2011).
[12] Y. Singh, S. Manni, J. Reuther, T. Berlijn, R. Thomale, W. Ku, S. Trebst, and P. Gegenwart, Phys. Rev. Lett. **108**, 127203 (2012).
[13] F. Ye, S. Chi, H. Cao, B. C. Chakoumakos, J. A. Fernandez-Baca, R. Custelcean, T. F. Qi, O. B. Korneta, and G. Cao, Phys. Rev. B **85**, 180403 (2012).
[14] R. Comin, G. Levy, B. Ludbrook, Z.-H. Zhu, C. N. Veenstra, J. A. Rosen, Y. Singh, P. Gegenwart, D. Stricker, J. N. Hancock, D. van der Marel, I. S. Elfimov, and A. Damascelli, Phys. Rev. Lett. **109**, 266406 (2012).
[15] A. Biffin, R. D. Johnson, I. Kimchi, R. Morris, A. Bombardi, J. G. Analytis, A. Vishwanath, and R. Coldea, Phys. Rev. Lett. **113**, 197201 (2014).
[16] A. Biffin, R. D. Johnson, S. Choi, F. Freund, S. Manni, A. Bombardi, P. Manuel, P. Gegenwart, and R. Coldea, Phys. Rev. B **90**, 205116 (2014).
[17] T. Takayama, A. Kato, R. Dinnebier, J. Nuss, H. Kono, L. S. I. Veiga, G. Fabbris, D. Haskel, and H. Takagi, Phys. Rev. Lett. **114**, 077202 (2015).
[18] S. Hwan Chun, J.-W. Kim, J. Kim, H. Zheng, C. C. Stoumpos, C. D. Malliakas, J. F. Mitchell, K. Mehlawat, Y. Singh, Y. Choi, T. Gog, A. Al-Zein, M. M. Sala, M. Krisch, J. Chaloupka, G. Jackeli, G. Khaliullin, and B. J. Kim, Nat. Phys. **11**, 462 (2015).
[19] S. C. Williams, R. D. Johnson, F. Freund, S. Choi, A. Jesche, I. Kimchi, S. Manni, A. Bombardi, P. Manuel, P. Gegenwart, and R. Coldea, Phys. Rev. B **93**, 195158 (2016).
[20] K. Kitagawa, T. Takayama, Y. Matsumoto, A. Kato, R. Takano, Y. Kishimoto, R. Dinnebier, G. Jackeli, and H. Takagi, Nature **554**, 341 (2018).
[21] K. W. Plumb, J. P. Clancy, L. J. Sandilands, V. V. Shankar, Y. F. Hu, K. S. Burch, H.-Y. Kee, and Y.-J. Kim, Phys. Rev. B **90**, 041112 (2014).
[22] J. A. Sears, M. Songvilay, K. W. Plumb, J. P. Clancy, Y. Qiu, Y. Zhao, D. Parshall, and Y.-J. Kim, Phys. Rev. B **91**, 144420 (2015).
[23] M. Majumder, M. Schmidt, H. Rosner, A. A. Tsirlin, H. Yasuoka, and M. Baenitz, Phys. Rev. B **91**, 180401 (2015).
[24] R. D. Johnson, S. C. Williams, A. A. Haghighirad, J. Singleton, V. Zapf, P. Manuel, I. I. Mazin, Y. Li, H. O. Jeschke, R. Valentí, and R. Coldea, Phys. Rev. B **92**, 235119 (2015).
[25] J. G. Rau, E. K.-H. Lee, and H.-Y. Kee, Phys. Rev. Lett. **112**, 077204 (2014).
[26] Y. Yamaji, Y. Nomura, M. Kurita, R. Arita, and M. Imada, Phys. Rev. Lett. **113**, 107201 (2014).
[27] Y. Sizyuk, C. Price, P. Wölfle, and N. B. Perkins, Phys. Rev. B **90**, 155126 (2014).
[28] I. Rousochatzakis, J. Reuther, R. Thomale, S. Rachel, and N. B. Perkins, Phys. Rev. X **5**, 041035 (2015).
[29] S. M. Winter, Y. Li, H. O. Jeschke, and R. Valentí, Phys. Rev. B **93**, 214431 (2016).
[30] V. M. Katukuri, R. Yadav, L. Hozoi, S. Nishimoto, and J. van den Brink, Sci. Rep. **6**, 29585 (2016).
[31] R. Yadav, N. A. Bogdanov, V. M. Katukuri, S. Nishimoto, J. van den Brink, and L. Hozoi, Sci. Rep. **6**, 37925 (2016).
[32] S. K. Choi, R. Coldea, A. N. Kolmogorov, T. Lancaster, I. I. Mazin, S. J. Blundell, P. G. Radaelli, Y. Singh, P. Gegenwart, K. R. Choi, S.-W. Cheong, P. J. Baker, C. Stock, and J. Taylor, Phys. Rev. Lett. **108**, 127204 (2012).
[33] J. Knolle, D. L. Kovrizhin, J. T. Chalker, and R. Moessner, Phys. Rev. Lett. **112**, 207203 (2014).
[34] J. Knolle, D. L. Kovrizhin, J. T. Chalker, and R. Moessner, Phys. Rev. B **92**, 115127 (2015).
[35] A. Smith, J. Knolle, D. L. Kovrizhin, J. T. Chalker, and R. Moessner, Phys. Rev. B **92**, 180408 (2015).
[36] A. Banerjee, C. A. Bridges, J.-Q. Yan, A. A. Aczel, L. Li, M. B. Stone, G. E. Granroth, M. D. Lumsden, Y. Yiu, J. Knolle, S. Bhattacharjee, D. L. Kovrizhin, R. Moessner, D. A. Tennant, M. D. G., and S. E. Nagler, Nature materials (2016), 10.1038/nmat4604.
[37] A. Smith, J. Knolle, D. L. Kovrizhin, J. T. Chalker, and R. Moessner, Phys. Rev. B **93**, 235146 (2016).
[38] X.-Y. Song, Y.-Z. You, and L. Balents, Phys. Rev. Lett. **117**, 037209 (2016).
[39] A. Banerjee, J. Yan, J. Knolle, C. A. Bridges, M. B. Stone, M. D. Lumsden, D. G. Mandrus, D. A. Tennant, R. Moessner, and S. E. Nagler, Science **356**, 1055 (2017).
[40] S.-H. Do, S.-Y. Park, J. Yoshitake, J. Nasu, Y. Motome, Y. Kwon, D. T. Adroja, D. J. Voneshen, K. Kim, T.-H. Jang, J.-H. Park, K.-Y. Choi, and S. Ji, Nat. Phys. **13**, 1079 (2017).
[41] J. Knolle, S. Bhattacharjee, and R. Moessner, Phys. Rev. B **97**, 134432 (2018).
[42] J. Knolle, G.-W. Chern, D. L. Kovrizhin, R. Moessner, and N. B. Perkins, Phys. Rev. Lett. **113**, 187201 (2014).
[43] L. J. Sandilands, Y. Tian, K. W. Plumb, Y.-J. Kim, and K. S. Burch, Phys. Rev. Lett. **114**, 147201 (2015).

[44] B. Perreault, J. Knolle, N. B. Perkins, and F. J. Burnell, Phys. Rev. B **92**, 094439 (2015).
[45] L. J. Sandilands, Y. Tian, A. A. Reijnders, H.-S. Kim, K. W. Plumb, Y.-J. Kim, H.-Y. Kee, and K. S. Burch, Phys. Rev. B **93**, 075144 (2016).
[46] A. Glamazda, P. Lemmens, S.-H. Do, Y. S. Choi, and K.-Y. Choi, Nat. Commun. **7**, 12286 (2016).
[47] B. Perreault, J. Knolle, N. B. Perkins, and F. J. Burnell, Phys. Rev. B **94**, 060408 (2016).
[48] B. Perreault, J. Knolle, N. B. Perkins, and F. J. Burnell, Phys. Rev. B **94**, 104427 (2016).
[49] Y. Wang, G. B. Osterhoudt, Y. Tian, P. Lampen-Kelley, A. Banerjee, T. Goldstein, J. Yan, J. Knolle, J. Nasu, Y. Motome, S. Nagler, D. Mandrus, and K. S. Burch, arXiv:1809.07782 (2018).
[50] G. B. Halász, N. B. Perkins, and J. van den Brink, Phys. Rev. Lett. **117**, 127203 (2016).
[51] G. B. Halász, B. Perreault, and N. B. Perkins, Phys. Rev. Lett. **119**, 097202 (2017).
[52] I. Rousochatzakis, S. Kourtis, J. Knolle, R. Moessner, and N. B. Perkins, arXiv:1811.01671 (2018).
[53] L. J. P. Ament, M. van Veenendaal, T. P. Devereaux, J. P. Hill, and J. van den Brink, Rev. Mod. Phys. **83**, 705 (2011).
[54] L. J. P. Ament, G. Khaliullin, and J. van den Brink, Phys. Rev. B **84**, 020403 (2011).
[55] L. Savary and T. Senthil, arXiv:1506.04752 (2015).
[56] B. J. Kim and G. Khaliullin, Phys. Rev. B **96**, 085108 (2017).
[57] T. Gog, D. Casa, A. Said, M. Upton, J. H. Kim, I. Kuzmenko, X. Huang, and R. Khachatryan, J. Synchrotron Radiat. **20**, 74 (2013).
[58] T. Gog, D. Casa, A. Said, M. Upton, J. H. Kim, I. Kuzmenko, X. Huang, and R. Khachatryan, `https://www.aps.anl.gov/Analyzer-Atlas/Analyzer-Atlas` (2016).
[59] J. Nasu, M. Udagawa, and Y. Motome, Phys. Rev. B **92**, 115122 (2015).
[60] J. Nasu, J. Knolle, D. L. Kovrizhin, Y. Motome, and R. Moessner, Nat. Phys. **12**, 912 (2016).
[61] J. Yoshitake, J. Nasu, and Y. Motome, Phys. Rev. Lett. **117**, 157203 (2016).
[62] J. Yoshitake, J. Nasu, Y. Kato, and Y. Motome, Phys. Rev. B **96**, 024438 (2017).
[63] J. Yoshitake, J. Nasu, and Y. Motome, Phys. Rev. B **96**, 064433 (2017).
[64] J. van den Brink, EPL (Europhysics Letters) **80**, 47003 (2007).
[65] A. J. Willans, J. T. Chalker, and R. Moessner, Phys. Rev. Lett. **104**, 237203 (2010).
[66] A. J. Willans, J. T. Chalker, and R. Moessner, Phys. Rev. B **84**, 115146 (2011).
[67] G. B. Halász, J. T. Chalker, and R. Moessner, Phys. Rev. B **90**, 035145 (2014).
[68] The first $1/\Gamma$ factor in Eq. (4) comes from the broadening of the resonant transition due to the short core-hole lifetime [see the denominator of Eq. (3)] and is generic to all RIXS processes in the fast-collision regime. The second $1/\Gamma$ factor comes from the time evolution in the short-lived intermediate state and is generic to all *indirect* RIXS processes in the fast-collision regime.
[69] A. Metavitsiadis, A. Pidatella, and W. Brenig, Phys. Rev. B **96**, 205121 (2017).
[70] Since M is a real matrix, U and V are real orthogonal matrices, while Λ is a diagonal matrix with non-negative (real) entries.
[71] W. J. Brya and P. M. Richards, Phys. Rev. B **9**, 2244 (1974).
[72] P. M. Richards and W. J. Brya, Phys. Rev. B **9**, 3044 (1974).
[73] G. F. Reiter, Phys. Rev. B **13**, 169 (1976).
[74] The integration *around* the Γ point is required because the RIXS intensity vanishes at the Γ point itself.
[75] Note, however, that the complete extinction of the RIXS intensity at the Γ point seen in Figs. 2 and 5 may be partially obscured in RIXS experiments, possibly appearing only as a suppression, due to the overlap with elastic scattering intensity, finite momentum resolution, or both.